Impact of Band Nonparabolicity and Interface Broadening effects on Electronic Structure and Rabi-Coupling Frequency in THz Quantum Cascade Lasers

Novak Stanojević, Aleksandar Demić, Nikola Vuković, Dragan Inđin and Jelena Radovanović

***Abstract*—Modeling of quantum cascade lasers requires precise determination of the emission frequency and current density for which the electronic band structure must be accurately solved. In this work, we explore the effect of the fourteenth-order k·p conduction band nonparabolicity and interface broadening due to inter-diffusion and fluctuations of the band edges on the electronic structure and Rabi-coupling oscillation frequency of a THz quantum cascade laser.**

***Index Terms*—QCL; nonparabolicity; interface broadening; anticrossing energy; Rabi oscillations.**

I. Introduction

Quantum cascade lasers (QCLs) [1] are unipolar semiconductor lasers with flexible emission wavelengths that can be engineered by variation of semiconductor layer thicknesses. Light emission occurs from the optical gain medium which consists of multiple quantum wells (QWs) in which quantized electron states (subbands) are formed. These electron subbands assume the role of the laser levels between which electron intersubband transitions occur. The frequency of the light emitted from the intersubband electron transitions in QCLs ranges from mid-infrared (mid-IR) to the THz part of the spectrum, i.e. the corresponding wavelengths vary typically from a few micrometers to a few hundred micrometers. QCLs were first demonstrated in 1994 [1] and their performance and emission frequency range has since been greatly improved. Continuous-wave (CW) operation has been achieved at room temperature (RT) for optical powers larger than 5 W in the range of 4.5-5 μm [2] and powers larger than 0.5 W for lowest wavelength QCL operation at 3.39 μm [3] in the mid-IR part of the spectrum. In the THz part of the spectrum, operation has been reported in the range of 1.2 THz to 5.6 THz. [4, 5, 6] and optical powers larger than 1 W have been achieved at cryogenic temperatures [7]. Pulsed operation has been achieved at 250 K [8] and CW operation at 129 K [9].

Through careful design of QCLs, the emission frequency can be altered by changing the layer thicknesses and QW barrier heights which results in the change of the bound state energies and wavefunctions. This process requires exact solving of the electronic band structure. The simplest theoretical model used for calculating the electronic band structure of QW structures is the single-band effective mass approximation. While this model gives good results in many cases, it does not take into account any form of nonparabolicity effects which could have a prominent influence on QCLs output characteristics, especially for the mid-IR range where electron bound states are high above the conduction band edge. In this work, we have also taken into account the interface broadening effects such as inter-diffusion and fluctuations of the band edges which change the material composition, to better describe the realistic growth of QCLs, and see what effect this has on the bound state energies and emission frequency.

QCLs consist of a large (typically $10 - 100$) number of repeated periods of multiple-QW structures. Each period can be approximately divided into an optical transition (optical gain) region and an injection/relaxation region. The gain region produces and maintains the population inversion between the two levels of the laser transition and is followed by the injection/relaxation region whose main purpose is to enable electron transport and injection by resonant tunneling into the upper laser level of the next period. The ground state in the first gain region is closely aligned with the upper laser level of the gain region in the following period of multi-QWs under an applied (resonant) electric field.

In the semiclassical model, intersubband scattering between these two subbands transports electrons from one eigenstate to another. These two levels form a doublet consisting of a lower-energy symmetric state, and a higher-energy antisymmetric state that are separated by an anticrossing energy gap Δ_{12}. Both of these states are spatially extended across the barrier and the transport through the barrier is effectively instantaneous, so the limiting factor for current density is the inelastic subband scattering between this doublet of states and the lower laser level of the following period. This leads to the current density being not directly dependent of the barrier thickness which is not valid for real devices.

Novak Stanojević is with the School of Electrical Engineering, University of Belgrade, 73 Bulevar kralja Aleksandra, 11020 Belgrade, Serbia (e-mail: novakstanojevic1@gmail.com) and with the Vlatacom Institute of High Technologies, 5 Bulevar Milutina Milankovića, 11070 Belgrade, Serbia (e-mail: novak.stanojevic@vlatacom.com).

Aleksandar Demić is with the School of Electronic and Electrical Engineering, University of Leeds, Leeds LS2 9JT, UK (e-mail: A.Demic@leeds.ac.uk), (https://orcid.org/0000-0003-1335-6156).

Nikola Vuković is with the School of Electrical Engineering, University of Belgrade, 73 Bulevar kralja Aleksandra, 11020 Belgrade, Serbia (e-mail: nvukovic@etf.bg.ac.rs), (https://orcid.org/0000-0002-4941-2546).

Dragan Inđin is with the School of Electronic and Electrical Engineering, University of Leeds, Leeds LS2 9JT, UK (e-mail: D.Indjin@leeds.ac.uk), (https://orcid.org/0000-0002-9121-9846)).

Jelena Radovanović is with the School of Electrical Engineering, University of Belgrade, 73 Bulevar kralja Aleksandra, 11020 Belgrade, Serbia (e-mail: radovanovic@etf.bg.ac.rs), (https://orcid.org/0000-0003-3031-7802).

 ISBN 978-86-7466-970-9

In a more physical model of transport, whose importance is described in detail in [10], electrons require a finite time to tunnel from one well to the next via the coherent time evolution of these states. The coherent superposition of the doublet energy states forms a wave packet that oscillates from one well to the other across the injection barrier at the Rabi-coupling oscillation frequency $\Omega_R = \Delta_{12}/\hbar$ with the wave packet being depleted when it is the right well by intersubband scattering. If pure dephasing is not taken into account the limiting factor for current density is the same as in the previous case. The most significant difference between this model and the semiclasical one occurs when taking into account dephasing scattering caused by elastic intrasubband scattering mechanisms such as interface roughness and electron-impurity scattering. Dephasing scattering dampens Rabi oscillation and can change the time evolution of the wave packet so much that it is no longer oscillatory, which causes the electrons to accumulate in the left well. This strong dephasing limit has been discussed in [11] and the limiting factor for the current density is the tunneling barrier, so the semiclassical model in which the electron distribution is uniform across the extended states is not appropriate for this case.

For mid-IR QCLs the injection barriers are relatively thin and the anticrossing gap Δ_{12} is large (~10-15 meV). Because of this, dephasing does not cause a significant oscillation damping and does not affect electron transport, so the semiclassical model is reasonably accurate. However THz QCLs have much thicker injection barriers and much smaller anticrossing gaps Δ_{12} (~1 meV), therefore dephasing scattering affects electron transport and the semiclassical model is inadequate and tends to overestimate the current density and material gain for particular values of applied electric field (terminal voltages) [12]. To adequately model these devices, we need to accurately solve the electronic structure and calculate the Rabi oscillation frequency. Therefore, in this work we investigate the effect of nonparabolicity and interface broadening on the electronic structure and Rabi oscillations in THz QCLs.

II. Theoretical Model

The conduction band dispersion relation of a bulk III-V material with a direct band gap was developed to the fourth order in the Ekenberg model which takes into account the interaction of the lowest conduction band with the light-hole and heavy-hole valence band, split-off band and three higher conduction bands [13]. The coefficients in the dispersion relation were calculated by solving the fourteenth order k·p model [14] and for 1D nanostructures this model results in the following form of the nonparabolic 1D effective mass Schrödinger equation which is used to obtain the electronic structure of the QCL:

$$\frac{d^2}{dz^2}\alpha_0(z)\frac{d^2\Phi_i(z)}{dz^2} - \frac{\hbar^2}{2}\frac{d}{dz}\frac{1}{m^*(z)}\frac{d\Phi_i(z)}{dz} + U_{eff}(z)\Phi_i(z) = E_i\Phi_i(z) \quad (1)$$

where $m^*(z)$ is the electron effective mass along the growth direction which varies with position due to the changes in material composition. The nonparabolicity parameter $\alpha_0(z)$ is also material dependent and quantifies the effect of nearby energy bands on the electron dispersion relation. $\Phi_i(z)$ is the wave function (envelope function), and E_i is the electron energy. $U_{eff}(z)$ is the total effective potential energy:

$$U_{eff}(z) = U_c(z) - eF_e z \quad (2)$$

which consists of the conduction band offset $U_c(z)$ between GaAs and AlAs, and the added bias potential energy due to the externally applied electric field F_e along the growth direction z.

The interfaces between different materials are often approximated by sharp step functions when electronic structure is calculated. However, due to inter-diffusion and fluctuations of the band edges realistic QCLs do not have such abrupt interfaces. These devices are typically made by epitaxial growth of a large number of layers composed of GaAs/AlGaAs, InGaAs/AlInAs, InAs/AlSb. Epitaxial growth is a stochastic industrial process prone to local variations in the chemical composition of the created ternary ($A_xB_{1-x}C$) alloys such as $Al_xGa_{1-x}As$ in GaAs/AlGaAs systems. Random diffusion of the charged dopants across the interface also leads to changes in the composition x. Both of these processes change the electronic behavior of the heterostructure.

It was shown [15] that modeling of interface broadening in an asymmetric double quantum well can be done in a simple analytical way by applying the phenomenological $\mathrm{tg}^{-1}(z)$ function instead of the Heaviside step function for describing the conduction band offset at the heterostructure interfaces. In this work we have used the same interface broadening function for a complex QCL structure, but instead of modeling the effective potential energy directly as in [15] we have applied the interface broadening function on the composition x which exactly describes the local variations of the composition in ternary alloys and diffusion of dopants at the interfaces.

$$x(z) = x_b\left(1 - \frac{1}{\pi}\sum\nolimits_j \mathrm{tg}^{-1}\left(\frac{z - Z_l}{\Gamma}\right) + \frac{1}{\pi}\sum\nolimits_j \mathrm{tg}^{-1}\left(\frac{z - Z_r}{\Gamma}\right)\right) \quad (3)$$

where Γ is the broadening parameter of the interfaces and x_b is the alloy composition in the barrier layers. The sum goes over all the well layers in the QCL structure where Z_l is the coordinate of the left interface (barrier/well layer interface) and Z_r is the coordinate of the right interface (well/barrier layer interface) for each well layer. By broadening the composition, we have not only described a more realistic conduction band offset $U_c(z)$, but also the effective mass along the growth direction $m^*(z)$ and the Ekenberg nonparabolicity parameter $\alpha_0(z)$ which are all functions of the alloy composition x.

Calculation of the anticrossing energy is needed to find the Rabi oscillation frequency $\Omega_R = \Delta_{12}/\hbar$. The anticrossing energy depends on the wavefunctions that form the energy doublet and between which the wave packet oscillates. In the tight binding model these wavefunctions, which are localized within one period are computed for each QCL period separately by solving the Schrödinger equation

 ISBN 978-86-7466-970-9

for the tight binding effective potential energy which consists only of one period and not for the total effective potential energy of the QCL which consists of all the periods. In practice it is only necessary to solve the electronic structure of one period and then the wavefunctions and bound state energies in the subsequent period can be found from [10]:

$$\phi_i^{(2)}(z) = \phi_i^{(1)}(z - l_p) \quad (4)$$

$$E_i^{(2)} = E_i^{(1)} + qV_{bias} \quad (5)$$

where l_p is the length of one period, q the electron charge and V_{bias} the applied bias voltage per one period. The anticrossing energy can then be found as [16]

$$\Delta_{12} = \sqrt{\left\langle \phi_i^{(1)} \middle| U_{eff} - U_{tb1} \middle| \phi_j^{(2)} \right\rangle \left\langle \phi_i^{(1)} \middle| U_{eff} - U_{tb2} \middle| \phi_j^{(2)} \right\rangle} \quad (6)$$

where U_{eff} is the total effective potential energy of the QCL which consists of all the periods, U_{tb1} and U_{tb2} are the tight binding effective potential energies for only the first and second QCL period respectively and $\phi_i^{(1)}$ and $\phi_j^{(2)}$ are the wavefunctions of the i-th and j-th states which form the energy doublet between which the resonant tunneling through the injection barrier occurs and which are localized in the first and second QCL period respectively.

III. Results and Discussion

In this section, we present the results of our numerical simulations. We have calculated the electronic structure of a THz QCL demonstrated in [17] by numerically solving the nonparabolic 1D effective mass Schrödinger equation (1) with the transfer matrix method (TMM) for one period of the QCL. This device employs a double quantum well (DQW) gain region and a thick injection barrier. The QCL design was implemented in GaAs/$Al_{0.15}Ga_{0.85}As$ and the thickness of the layers starting from the injector barrier in Å are **56**/71/**31**/167 where the thicknesses of the barrier layers are bolded. The design bias was 17 kV/cm while the n-doping of the injector well (underlined thickness) was uniform with the effective 2D carrier density being $2.17 * 10^{10}$ cm^{-2} per period.

In Fig. 1. we see the effective potential energy of one period of the QCL with no interface broadening. There are four bound energy states with their corresponding wavefunctions squared (probability densities). Electrons are injected into the upper laser level (state 3) by resonant tunneling. The radiative transition between state 3 (purple) and state 2 (yellow) produces the optical gain, while the lower laser level (state 2) is depopulated by fast intrawell electron-longitudinal-optical phonon scattering into the injector state 1 (orange) [17].

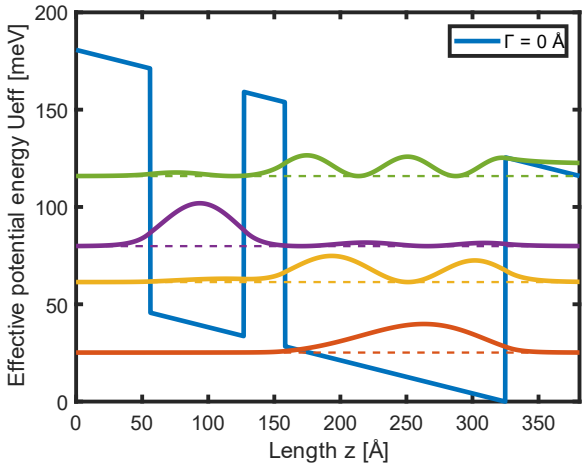

Fig. 1. The effective potential energy of one period of the QCL with bound energy states and their corresponding wavefunctions squared shown without interface broadening effects.

Using the electronic structure of one period of the QCL and equations (4) and (5) the structure with two periods was created. Fig. 2. shows the effective potential energy, bound state energies and the corresponding wavefunctions squared for two periods of the QCL where interface broadening effects are taken into account and the broadening parameter Γ is equal to 0.5 Å. For simplicity, only the first three quasi bound states are shown in each period. Resonant tunneling through the injection barrier occurs between state 1 (green) in the left period and state 3 (purple) in the right period.

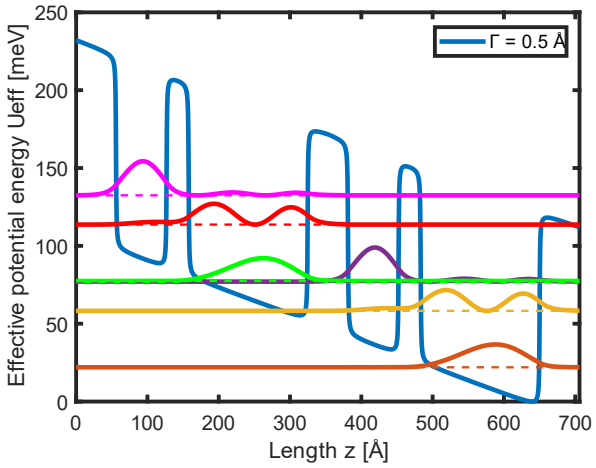

Fig. 2. The effective potential energy of two periods of the QCL with bound energy states and their corresponding wavefunctions squared shown.

We varied the interface broadening parameter in order to see the effect it has on the electronic structure of the QCL. In Fig. 3. we can see that the energy of all four energy subbands decreases with the increase of the broadening parameter. This effect occurs owing to the well layers effectively becoming wider at the top and narrower at the bottom of the conduction band offset, which also affects the electron effective mass and the nonparabolicity parameter.

 ISBN 978-86-7466-970-9

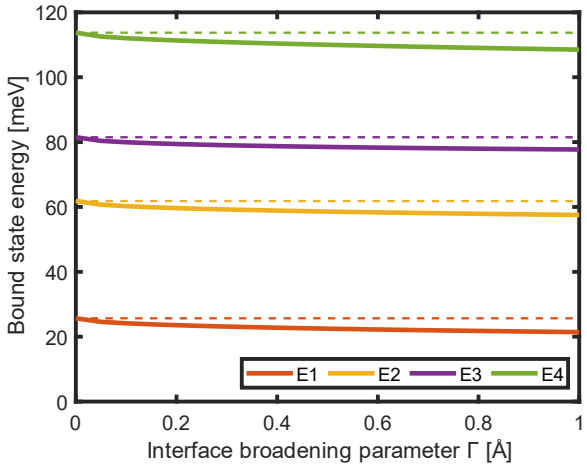

Fig. 3. The energy of the four bound states as a function of the interface broadening parameter with nonparabolicity taken into account.

In order to see what effect nonparabolicity has on the electronic structure, emission frequency, and Rabi oscillation frequency we have also solved 1D effective mass Schrödinger equation without including nonparabolicity effects ($\alpha_0(z) = 0$).

Light emission from the gain region is due to the radiative transition from state 3 to state 2 in each period. The frequency of this transition can be found as $\nu = (E_3 - E_2)/h$. The emission frequency of a QCL is one of its most important characteristics, and for real-life applications, it is often necessary to calculate it with high accuracy, which requires taking into account nonparabolicity and interface broadening effects. We see in Fig. 4. that when the nonparabolicity is taken into account the emission frequency of the QCL shifts to larger values and that in both cases it increases with the increase of the interface broadening parameter.

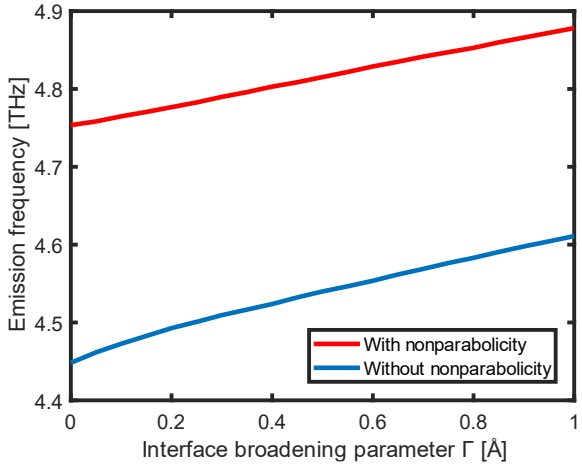

Fig. 4. The emission frequency of the QCL as a function of the interface broadening parameter.

The Rabi oscillation frequency is found by calculating the anticrossing energy (6) between the resonant states (denoted by the green and purple lines in Fig. 2.) and dividing it by the reduced Planck constant $\Omega_R = \Delta_{12}/\hbar$. It can be seen from (6) that the anticrossing energy depends only on the region of the structure where the resonant states overlap that is the injection barrier.

Accurate determination of the Rabi frequency is especially important for THz QCLs with a single thick injection barrier because for these structures dephasing scattering affects electron transport and the limiting factor for the current density can be the Rabi frequency. In Fig. 5. we show how the Rabi frequency depends on the interface broadening parameter for both cases.

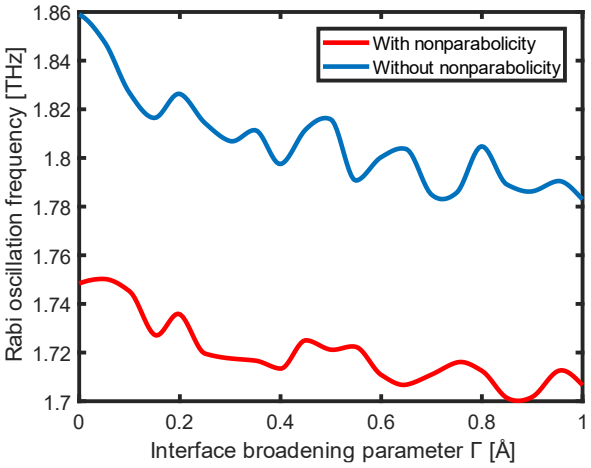

Fig. 5. The Rabi oscillation frequency of the QCL as a function of the interface broadening parameter.

In Table 1. we present the energy of the bound states of both calculations for a structure without interface broadening effects ($\Gamma = 0$ Å). We can see that the shift in the energy of the bound states is larger for higher states.

TABLE I
EFFECT OF NONPARABOLICITY ON THE ELECTRONIC STRUCTURE

	E_1[meV]	E_2[meV]	E_3[meV]	E_4[meV]
With nonparabolicity	25,7	61,8	81,5	113,7
Without nonparabolicity	25,2	61,4	79,9	115,9

IV. CONCLUSION

In this work we have analyzed the effect of interface broadening modeled in a simple analytical way by applying the phenomenological $\mathrm{tg}^{-1}(z)$ function on the chemical composition of the layers at each interface and the effect of the fourteenth order k·p nonparabolicity model for the conduction band on the electronic structure and Rabi oscillation frequency of a THz QCL.

The results presented in this paper show that for modeling real devices with precise required emission frequencies interface broadening and band nonparabolicity must be taken into account because of their effect on the bound state energies and in turn the emission frequency. While for those QCLs, where the limiting factor for the current density is the Rabi frequency, it needs to be accurately calculated as it affects the current density and material gain of the QCL.

 ISBN 978-86-7466-970-9

ACKNOWLEDGMENT

This work was financially supported by the Ministry of Science, Technological Development and Innovation of the Republic of Serbia under contract number: 451-03-47/2023-01/200103, "Multi-Scale Modeling of Terahertz Quantum Cascade Laser Active Regions", Multilateral scientific and technological cooperation in the Danube region 2020-2021, "DEMETRA: Development of high-performance mid-IR / THz quantum cascade lasers for advanced applications", Science Fund of the Republic of Serbia, Serbian Science and Diaspora Collaboration Programme: Knowledge Exchange Vouchers, and European Cooperation in Science and Technology (COST) Action CA21159 PhoBioS.

REFERENCES

[1] J. Faist, F. Capasso, D. L. Sivco, C. Sirtori, A. L. Hutchinson, and A. Y.Cho, "Quantum cascade laser," Science 264, 553 (1994).

[2] Y. Bai, N. Bandyopadhyay, S. Tsao, S. Slivken, and M. Razeghi, "Room temperature quantum cascade lasers with 27% wall plug efficiency," Appl. Phys. Lett. 98, 181102 (2011).

[3] N. Bandyopadhyay, S. Slivken, Y. Bai, and M. Razeghi, "High power, continuous wave, room temperature operation of $\lambda \sim 3.4$ μm and $\lambda \sim 3.55$ μm InP-based quantum cascade lasers," Appl. Phys. Lett. 100, 212104 (2012).

[4] S. Kumar, "Recent progress in terahertz quantum cascade lasers," IEEE J. Sel. Top. Quantum Electron. 17(1), 38 (2011).

[5] S. Kumar, Q. Hu, and J. L. Reno, "186 K operation of terahertz quantumcascade lasers based on a diagonal design," Appl. Phys. Lett. 94, 131105 (2009).

[6] M. Wienold, B. Roben, X. Lu, G. Rozas, L. Schrottke, K. Biermann and H. T. Grahn, "Frequency dependence of the maximum operating temperature for quantum-cascade lasers up to 5.4 THz," Appl. Phys. Lett. 107 202101 (2015).

[7] L. Li, L. Chen, J. Zhu, J. Freeman, P. Dean, A. Valavanis, A. G. Davies and E. H. Linfield, "Terahertz quantum cascade lasers with >1 W output powers," Electron. Lett. 50 309–311 (2014).

[8] A. Khalatpour, A. K. Paulsen, C. Deimert, Z. R. Wasilewski and Q. Hu, "High-power portable terahertz laser systems," Nat. Photon. 15 16–20 (2021).

[9] M. Wienold, B. Roben, L. Schrottke, R. Sharma, A. Tahraoui, K. Biermann and H. T. Grahn, "High-temperature, continuous-wave operation of terahertz quantum-cascade lasers with metal–metal waveguides and third-order distributed feedback," Opt. Express 22 3334–48 (2014).

[10] H. Callebaut and Q. Hu, "Importance of coherence for electron transport in terahertz quantum cascade lasers," *J. Appl. Phys.*, vol. 98, 104505 (2005).

[11] S. Luryi, "Frequency limit of double-barrier resonant-tunneling oscillators, " Appl. Phys. Lett. 47, 490 (1985).

[12] A. Demić, A. Grier, Z. Ikonić, A. Valavanis, C. A. Evans, R. Mohandas, L. Li, E. H. Linfield, A. G. Davies and D. Indjin, "Infinite-period density-matrix model for terahertz-frequency quantum cascade lasers," IEEE Transactions on Terahertz Science & Technology, 7 (4). pp. 368-377 (2017).

[13] U. Ekenberg, "Nonparabolicity effects in a quantum well:Sublevel shift, parallel mass, and Landau levels," Physical Review B 40,7714 (1989).

[14] M. Braun and U. Rössler, "Magneto-optic transitions and non-parabolicity parameters in the conduction band of semiconductors," J. Phys. C 18, 3365 (1985).

[15] V. Gavryushin, "Asymmetric double quantum wells with smoothed interfaces," centr.eur.j.phys. 10, 459–469 (2012).

[16] A. Yariv, C. Lindsey, and U. Sivan, "Approximate analytic solution for electronic wave functions and energies in coupled quantum wells," J. Appl. Phys., vol. 58, no. 9, pp. 3669–3672, (1985).

[17] S. Kumar, C. W. I. Chan, Q. Hu, and J.L. Reno, "Two-well terahertz quantum-cascade laser with direct intrawell-phonon depopulation," Appl. Phys. Lett. 95, 141110 (2009).

 ISBN 978-86-7466-970-9